

3D Printed Parts with Honeycomb Internal Pattern by Fused Deposition Modelling; Experimental Characterization and Production Optimization

Moradi, M., Meiabadi, S. & Kaplan, A.

Author post-print (accepted) deposited by Coventry University's Repository

Original citation & hyperlink:

Moradi, M, Meiabadi, S & Kaplan, A 2019, '3D Printed Parts with Honeycomb Internal Pattern by Fused Deposition Modelling; Experimental Characterization and Production Optimization', *Metals and Materials International*, vol. 25, no. 5, pp. 1312-1325.

DOI 10.1007/s12540-019-00272-9

ISSN 1598-9623

ESSN 2005-4149

Publisher: Springer

The final publication is available at Springer via <http://dx.doi.org/10.1007/s12540-019-00272-9>

Copyright © and Moral Rights are retained by the author(s) and/ or other copyright owners. A copy can be downloaded for personal non-commercial research or study, without prior permission or charge. This item cannot be reproduced or quoted extensively from without first obtaining permission in writing from the copyright holder(s). The content must not be changed in any way or sold commercially in any format or medium without the formal permission of the copyright holders.

This document is the author's post-print version, incorporating any revisions agreed during the peer-review process. Some differences between the published version and this version may remain and you are advised to consult the published version if you wish to cite from it.

3D Printed Parts with Honeycomb Internal Pattern by Fused Deposition Modelling; Experimental Characterization and Production Optimization

Mahmoud Moradi*^a, Saleh Meiabadi^b, Alexander Kaplan^c

^a Department of Mechanical Engineering, Faculty of Engineering, Malayer University, Malayer, Iran

^b Department of Mechanical Engineering, École de Technologie Supérieure, Canada 1100 Notre-Dame West, Montreal, QC, H3C 1K3, Canada.

^c Department of Engineering Sciences and Mathematics, Lulea University of Technology, 971 87, Lulea, Sweden

* Corresponding Author: moradi.malayeru@gmail.com (Mahmoud Moradi)

Abstract

In the present study additive manufacturing of Polylactic acid (PLA) by fused deposition modeling (FDM) were investigated based on statistical analysis. The honeycomb internal pattern was employed to build inside of specimens due to its remarkable capability to resist mechanical loads. Simplify 3D was utilized to slice the 3D model and to adjust fixed parameters. Layer thickness, infill percentage, and extruder temperature were considered as controlled variables, while maximum failure load (N), elongation at break (mm), part weight (gr), and build time (min) were selected as output responses and analysed by response surface method. Analysis of variance results identified layer thickness as the major controlled variable for all responses. Interaction of infill percentage and extruder temperature had a significant influence on elongation at break and therefore, tough fracture of printed parts. The input parameters were optimized to materialize tow criteria; the first one was to rise maximum failure load and the second was to attain tough fracture and lessen build time and part weight at a time. Optimal solutions were examined by experimental fabrication to evaluate the efficiency of the optimization method. There was a good agreement between empirical results and response surface method predictions which confirmed the reliability of predictive models. The optimal setting to fulfill the first criterion could bring on a specimen with more than 1500 (N) maximum failure load and less than 9 (gr) weight.

Keywords: 3D Printing; Fused Deposition Modelling; Mechanical properties; Part weight; Response Surface Method.

1. Introduction

Rapid Prototyping (RP) technologies are gradually developing to rapid manufacturing (RM) technologies due to widespread applications of rapid prototyping technologies in various industries. Nowadays, applications for additive manufacturing (AM) methods are growing in different fields namely industrial, medical, and architectural sectors. Additive manufacturing technologies build 3D components by adding successive layers of feedstock material that fuse together to create consolidated components. Fused deposition modeling (FDM) is a rapid prototyping process in which a filament of wax or polymer is extruded onto the existing part surface from a workhead to complete each new layer [1]. FDM works best with polymers that are amorphous in nature rather than highly crystalline polymers. This is because polymers that work best are those that are in a viscous paste rather than in a lower viscosity form. As amorphous polymers, there is no distinct melting point, and the material increasingly softens, and viscosity lowers with increasing temperature [2].

Many researchers investigated FDM process parameters by design of experiments method [3, 4, 5, 6], and many others evaluated the FDM process by evolutionary algorithm or artificial intelligence techniques [7, 8, 9, 10]. According to the literature, Padhi et al. [11] investigated effects of several process parameters including layer thickness, raster angle, raster width, air gap, part orientation, and their interactions on the accuracy of the length, width, and thickness, of acrylonitrile-butadiene-styrene (ABSP 400) parts fabricated through FDM technique. The process parameters were optimized to minimize the outputs responses, such as the change in length, width, and thickness of the test specimen by Taguchi method. Taguchi's philosophy was not able to reach uniform optimal factor settings for each response. Therefore, a combined method of a fuzzy inference system and Taguchi philosophy were implemented to create a single response for three responses to attain overall optimum factor level settings. Gardan et al. [12] presented a new filament deposition for fused deposition modeling. Several specimens were printed to evaluate fracture behaviour of specimens. The new filament could result in a 30% improvement in the toughness of specimens. A ductile-like behavior associated with large deformation zone was achieved by modifying the filament direction. Peng et al. [13] studied the effects of line width compensation, extrusion velocity, filling velocity, and layer thickness on the dimensional error, warp deformation, and built time. The three responses were converted to a single output by a fuzzy inference system. The response surface methodology (RSM) was used to determine the relationship between four input parameters and a comprehensive output. Matlab software was also used to implement fitness function in the genetic algorithm. Results showed that the proposed method in could effectively improve accuracy and efficiency in the FDM process. Sajan et al. [14] conducted a study to improve circularity and surface finish of a grinder blade of acrylonitrile butadiene styrene (ABS). The part had three holes in three plains. Bed temperature, nozzle temperature, print speed, infill percentage, layer thickness and a number of loops were considered as input parameters. Taguchi method was performed to reach optimum process parameters to improve circularity and surface roughness. Results indicated that circularity error and surface roughness were minimum at the hole printed in XY plane and maximum at XZ plane. Gautam et al. [15] investigated the compressive performance of ABS Kagome truss unit cell fabricated by fused deposition modeling. Effects of part build orientation, the diameter of the strut, the height of the core and the surface roughness on the peak strength and the effective stiffness were studied. It was found that the average peak strength and effective stiffness varies by 23% and 19% with different build orientation

due to changes in strut dimensions with different build direction as well as the anisotropic compressive behavior of FDM printed parts. The numerical results of effective stiffness differed from experimental measurements by 10–17% attributed to the imperfections like voids and staircase surfaces on the struts.

Ning et al. [16] investigated the mechanical properties of CFRP composites part manufactured by FDM. The first step of the investigation was to produce CFRP composites filaments by adding carbon fiber to plastic materials. The second step printing specimens by FDM. The third step was to conduct the tensile test. The composite filament resulted in increasing tensile strength and Young's modulus. However, toughness, ductility, and yield strength were decreased using a composite filament.

Additive manufacturing displays significant potential for replacement of traditionally manufactured parts, part repair, and prototype, however, properties of parts processed through additive typically suffer in comparison [17]. Opportunities for 3D printing nanostructures materials are investigated to improve the properties of the final printed part [18]. Mechanical properties can be increased through adjustment of FDM processing parameters such as build speed, build direction about the part orientation, layer thickness, and fill pattern comparison [17]. Also, a key requirement of any materials to be used in FDM is compatibility of the material with existing FDM setup without changing functional hardware/software of the machine [19]. In the current research, PLA tensile test sample was used to study effects of layer thickness, infill percentage, extruder temperature and their interactions on mechanical properties, build time, and part weight by design of experiment (DOE) method. PLA presents relatively brittle behaviour under tensile loading. The main objective of this study is to fine tune controlled variables to produce tough PLA specimen, reduce part weight, and lessen build time of the printed parts. Also, the honeycomb internal fill pattern was implemented to boost mechanical performance and decrease material consumption. Interior solidity of the printed parts can also be established by infill percentage. The build time data were measured after printing the specimens by a digital timer, and the parts weight were measured by a weighing scale. The tensile test determined the maximum failure load and elongation at break. Design-Expert V8 software was exploited to statistical analysis of experimental data via response surface method (RSM). The research objective was accomplished by RSM and validated by experimental fabrication. Validation of the statistical model was confirmed by getting the analogous results to experimental data.

2. Experimental Design and Methodology

2.1. Response Surface Method

It is of great significance to fine-tune variety of build parameters to optimize properties of 3D printed parts. Response surface methodology (RSM) is a structured and arranged method to identify relationships between factors affecting a process and output of the process [20]. RSM is advantageous to quantify relationships between output parameters and vital input factors. The aim is to determine a relationship between outputs and inputs with a minimum error in the form of a mathematical model. [21]. A functional relationship relating a response η with k levels of controlled variables is [22]:

$$\eta = f(x_1, x_2, \dots, x_k) + \mathcal{E} \quad (1)$$

Where \mathcal{E} represents the random experimental error due to some unknown or uncontrollable variables. To optimize the response η , it is necessary to find a suitable approximation for the true functional relationship between the independent variables

and the response surface [23]. The second order polynomial equation was used for representing the response and also expressed in the form of equation (2):

$$\eta = \beta_0 + \sum_{i=1}^k \beta_i x_i + \sum_{i=1}^k \beta_{ii} x_i^2 + \sum_{i,j=1}^k \sum_{i<j} \beta_{ij} x_i x_j \quad (2)$$

In equation 2, β_0 is constant, β_i is linear coefficients, β_{ii} is coefficients of quadratic, β_{ij} is interaction coefficients, and ε is the error of parameters of regression. In this study layer thickness, infill percentage, and extruder temperature were considered as controlled variables. The statistical analysis was performed on experimental data by Design-Expert V8 software. The statistical analysis was designed based on Central Composite Design (CCD) full replication with three factors five levels. Table 1 shows levels of controlled factors. Coding reduces the range of each factor to a common scale, -2 to +2, regardless of its relative magnitude. Maximum failure load (N), elongation at break (%). Part weight (gr), and build time (min) opted as output responses. The designed experiments and results of experiments are shown in Table 2.

Table 1. Levels of independent variables

Variable	Symbol	Unit	Levels				
			-2	-1	0	1	2
Layer Thickness	LT	mm	0.1	0.15	0.2	0.25	0.3
Infill Percentage	IP	%	10	20	30	40	50
Extruder Temperature	ET	C	190	200	210	220	230

Table 2. Design matrix and experiments results

Run	Input Variables			Output Responses				Type of Fracture
	Layer Thickness (LT)	Infill Percentage (IP)	Extruder Temperature (ET)	Maximum Failure Load (N)	Elongation at break (mm)	Part Weight (gr)	Build Time (min)	
1	0.20	30.00	210.00	1263	3.1294	7.92	35	Brittle
2	0.20	30.00	210.00	1238.5	2.5069	7.86	35	Brittle
3	0.15	40.00	220.00	1079.1	2.4006	7.52	43	Brittle
4	0.30	30.00	210.00	1496	5.6586	9.14	27	Tough
5	0.20	30.00	210.00	1054.6	3.1281	7.88	35	Brittle
6	0.25	40.00	200.00	1336.6	6.2812	8.72	31	Tough
7	0.25	20.00	200.00	1324.4	3.0758	8.37	30	Brittle
8	0.15	20.00	220.00	1201.7	3.6945	6.92	40	Brittle
9	0.20	30.00	210.00	1189.5	5.7852	7.83	35	Tough
10	0.15	40.00	200.00	1226.3	2.7683	7.56	43	Brittle
11	0.20	30.00	210.00	1066.8	2.4134	7.87	35	Brittle
12	0.20	10.00	210.00	1164.9	2.8005	7.45	33	Brittle
13	0.10	30.00	210.00	711.2	2.7617	6.45	54	Brittle
14	0.15	20.00	200.00	870.6	2.1663	6.97	40	Brittle
15	0.20	30.00	230.00	1385.7	3.7018	7.94	34	Brittle
16	0.20	30.00	190.00	1189.5	3.4015	7.85	34	Brittle
17	0.20	50.00	210.00	1410.2	3.5957	8.40	36	Brittle
18	0.25	40.00	220.00	1515.1	5.1222	8.91	31	Tough
19	0.25	20.00	220.00	1459.2	5.8019	8.59	30	Tough
20	0.20	30.00	210.00	1214	2.6181	7.88	35	Brittle

2.2. Experimental Work

Poly(lactic acid) or poly(lactide) (PLA) is a biodegradable and bioactive polyester made up of lactic acid building blocks. It is the default filament of choice for most extrusion-based 3D printers because it can be printed at a low temperature and does not require a heated bed. PLA is easy to print, very inexpensive, and creates parts that can be used for

a wide variety of applications. It is also one of the most environmentally friendly filaments on the market today, renewable and most importantly biodegradable. However, PLA has a limitation due to its inherent brittleness [24]. Table 3 shows the properties of PLA.

Table 3. Material properties.

<i>Property</i>	<i>Value</i>
<i>Full Name</i>	Polylactic acid (PLA)
<i>Melting Point</i>	150 to 160 °C (302 to 320 °F)
<i>Glass Transition</i>	60-65 °C
<i>Injection Mold Temperature</i>	178 to 240 °C (353 to 464 °F)
<i>Density</i>	1.210–1.430 g·cm ⁻³
<i>Chemical Formula</i>	(C ₃ H ₄ O ₂) _n
<i>Crystallinity</i>	37%
<i>Tensile Modulus</i>	2.7–16 GPa

3D printing of PLA was conducted by fused deposition modeling (FDM) method. Simplify3D software was used to adjust build parameters of specimens. Simplify3D includes an incredibly realistic pre-print simulation that allows seeing the exact performance of the 3D printer before starting the print. The simulation includes information about the exact speeds, sequences, and settings that are used for the print. The tensile test sample was designed based on international standard ISO 527-2 by Solidwork software and imported in Simplify3D. Table 4 illustrates definitions of FDM build parameters.

Table 4. FDM build parameters

No	Build Parameters	Definition
1	Nozzle diameter	The diameter of the extruder nozzle.
2	Extrusion width	The desired single-outline width of the plastic extrusion.
3	Build orientation	The angle between the main axis of the part and the horizontal direction
4	Top solid layer	Number of solid layers to require at the top of the part.
5	Bottom solid layers	Number of solid layers to require at the bottom of the part.
6	Default printing speed	Initial speed used for all printing movements (modification may be added for cooling or outline underspeed).
7	Retraction speed	Extruder speed for the retraction movements, typically uses the highest speed the extruder can support.
8	Outline overlap	Percentage of extrusion width that will overlap with outline perimeters (ensures infill bonds to outline).
9	Interior fill percentage	Determines the interior solidity of the model.
10	Extruder temperature	Defines the temperature at each build layer.

According to Table 2 which is designed based on a design of experiments, 20 samples were printed in different settings to investigate the effect of input parameters, mentioned in Table 1, on the quality of 3D printed specimens. In FDM 3D printing build orientation is considered 45° for the solid surface of specimens. Honeycomb pattern can be seen in many natural and industrial structures which introduces its solidity against mechanical loads and ability to redistribute localized stresses. Honeycomb structures are frequently utilized in the aerospace industry and many other fields due to its strength. Therefore, honeycomb internal fill pattern was used for the interior part of specimens to enhance loading capacity of specimens. Different honeycomb infill percentages are represented in Fig. 2. Geometrical dimensions and internal pattern of the sample are demonstrated in Fig. 3. Table 5 displays fixed parameters which are permanent for all experiments.

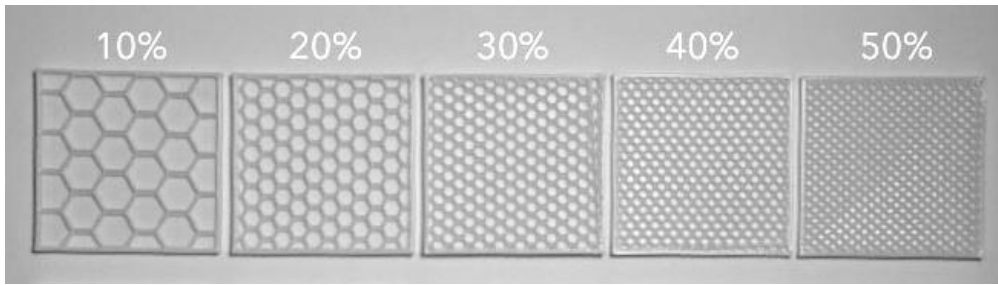
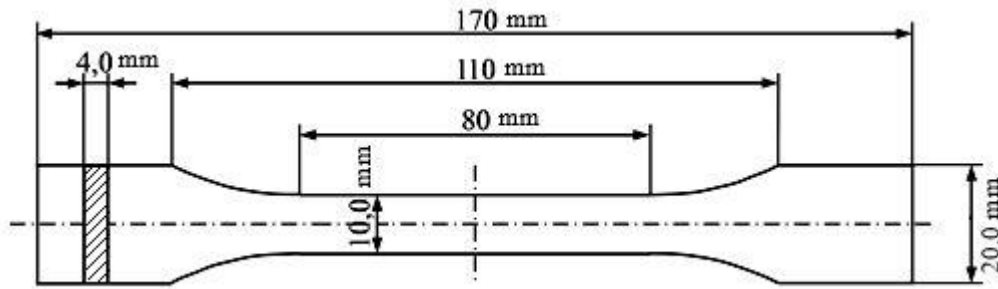


Fig. 2. Honeycomb infill percentages (10% to 50%).



(a)



(b)

Fig. 3. Geometrical dimensions and internal features of the sample (a) dimensions of the tensile test sample according to ISO 527-2 (b) % 30 full honeycomb infill percentage

Table 5. Values of fixed factors

<i>Variable</i>	<i>Unit</i>	<i>Value</i>
<i>Nozzle Diameter</i>	Mm	0.45
<i>Extrusion Width</i>	Mm	0.45
<i>Build orientation</i>	Degree	45
<i>Top Solid Layer</i>	-	6
<i>Bottom Solid Layer</i>	-	6
<i>Default Printing Speed</i>	mm/min	3600
<i>Retraction Speed</i>	mm/min	1800
<i>Internal Fill Pattern</i>	-	Full Honeycomb
<i>Outline Overlap</i>	%	15

The build time was measured after printing of each specimen by a digital timer; part weight was measured via a precise weighing scale; maximum failure load and elongation at break were acquired by the tensile test. The tensile tests were performed by a universal testing machine based on ASTM D638. Results indicated that the behaviour of specimens under load could be classified as the brittle and tough fracture. Almost 80% of outputs in the design matrix are showing brittle fracture because PLA is relatively brittle under tensile loading. The fracture of brittle specimens took place at the elastic limit, while tough specimens exhibited the ability to undergo a slight measure of plastic deformation before the break. Therefore, specimens with higher maximum failure load and elongation at break denoted tough fracture. However, the sudden brittle fracture was usually observed in specimens at elastic limit and in lower failure load. Brittle fracture of a specimen on the universal testing machine is shown in Fig. 4. Figure 5 represents Extension-Force diagrams of a tough and brittle specimen.



Fig. 4. Brittle fracture of the specimen (sample #12)

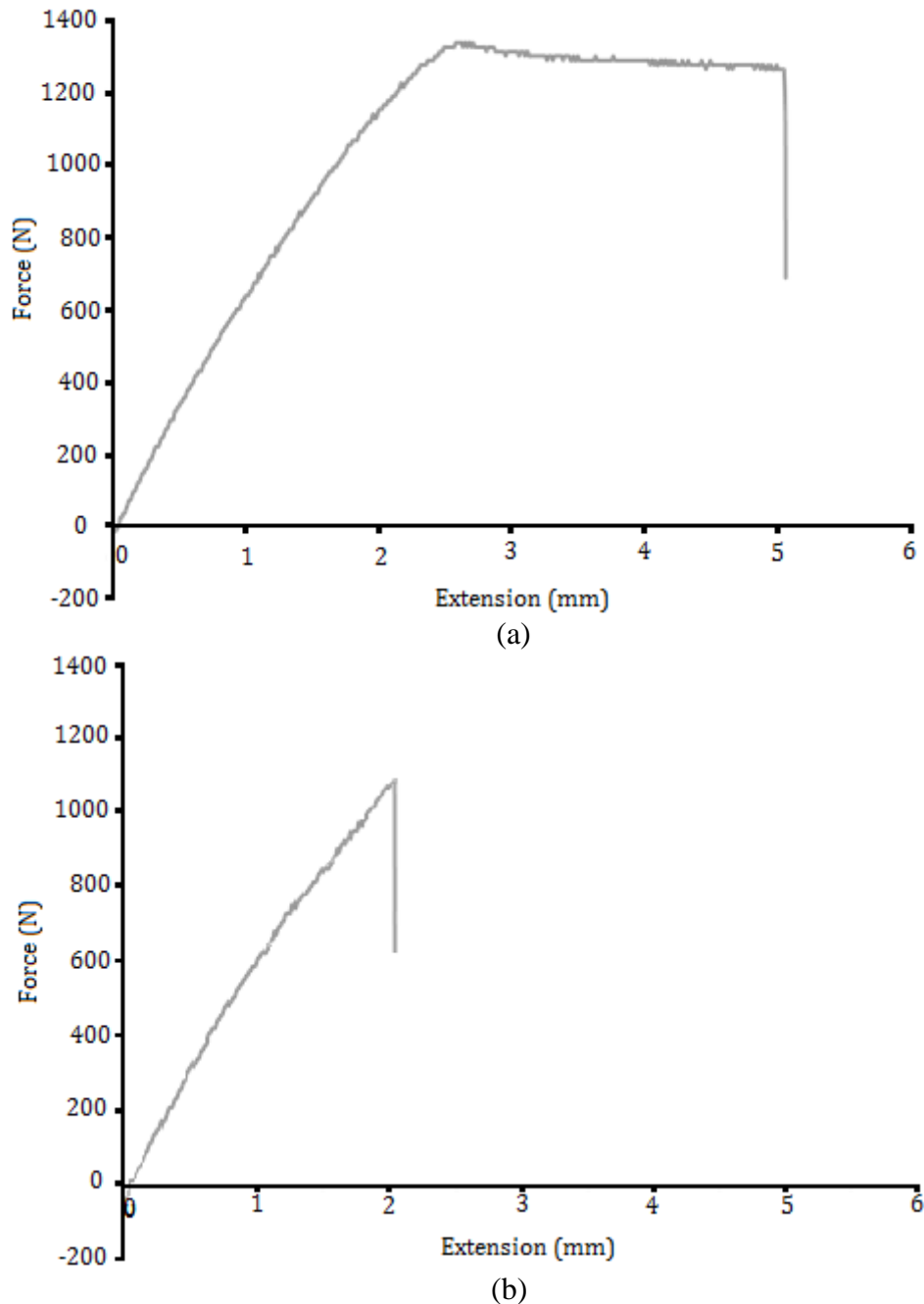


Fig. 5. Extension-Force diagrams of (a) tough specimen (sample # 6) and (b) brittle specimen (sample # 12)

3. Results and Discussion

The analysis of variance (ANOVA) reveals the effects of independent variables on output responses. The ANOVA is built entirely on the premise that factors are fixed, not random, and the design is crossed, not nested. The program calculates effects for all model terms. It produces statistics such as p-values, lack of fit, and R-squared values for comparing models. F-Values imply that models are significant and these models can be used to study the design space. In the mathematical model, the software selects higher polynomial where additional terms are significant, and the model is not aliased. Design-Expert offers a guideline to select a correct power law transformation. It is useful to determine the most appropriate power transformation to apply to response data.

3.1. Maximum Failure Load

ANOVA table reveals that layer thickness is the dominant controlled variable for maximum failure load. Extruder temperature and infill percentage are also significant. Table 6 demonstrates the ANOVA results of maximum failure load.

Table 6. Analysis of variance (ANOVA) for maximum failure load

<i>Source</i>	<i>Sum of Squares</i>	<i>Df</i>	<i>Mean Square</i>	<i>F Value</i>	<i>p-value</i>
<i>Model</i>	6.335E+015	3	2.112E+015	20.52	< 0.0001
<i>Layer Thickness(LT)</i>	5.153E+015	1	5.153E+015	50.06	< 0.0001
<i>Infill Percentage(IP)</i>	4.973E+014	1	4.973E+014	4.83	0.0430
<i>Extruder Temperature(ET)</i>	6.848E+014	1	6.848E+014	6.65	0.0202
<i>Residual</i>	1.647E+015	16	1.029E+014		
<i>Lack of Fit</i>	1.268E+015	11	1.153E+014	1.52	0.3375
<i>Pure Error</i>	3.791E+014	5	7.582E+013		
<i>Cor Total</i>	7.982E+015	19			
Adj R-Squared		0.7550	R-Squared	0.7937	

Equation (3) is predictive model of maximum failure load in terms of coded factors:
 $(\text{Maximum Failure Load})^{2.5} = +5.465\text{E}+007 + 1.795\text{E}+007 \text{ LT} + 5.575\text{E}+006 \text{ IP} + 6.542\text{E}+006 \text{ ET}$ (3)

Equation (4) is predictive model of maximum failure load in terms of actual values:
 $(\text{Maximum Failure Load})^{2.5} = -1.71241\text{E}+008 + 3.58918\text{E}+008 \text{ LT} + 5.57518\text{E}+005 \text{ IP} + 6.54222\text{E}+005 \text{ ET}$ (4)

The coded equation is worthwhile to determine the relative significance of factors by comparing the factor coefficients. Figure 6 depicts the perturbation plot of maximum failure load. The perturbation plot helps to compare the effect of all factors in the central point in the design space which is shown in the figure. The maximum failure load is plotted by changing only one factor over its range while holding other factors constant. Lines A, B, and C show sensitivity of maximum failure load to the layer thickness, infill percentage, and extruder temperature respectively. The perturbation plot discloses increasing all input parameters results in increasing mechanical strength of specimens. However, layer thickness has much more influence. Also, the plot reveals that maximum failure load is almost equally sensitive to extruder temperature and infill percentage. Figure 7 demonstrates effects of layer thickness and infill percentage on maximum failure load. 3D surface plot of maximum failure load in terms of layer thickness and extruder temperature is displayed in Fig. 8. Figure 9 indicates the normal probability plot of the studentized residuals to check for normality of residuals. The normal probability plot indicates whether residuals follow a normal distribution; in this case, the points follow a straight line. Some moderate scatter even with normal data is expected.

By increasing layer thickness the part thickness (4 mm) is divided into the fewer number of sections, and therefore the specimen printed by a thicker layer consists of less interlayer adhesion than a specimen with a thinner layer. Therefore, increasing layer thickness directly results in less interlayer adhesion. Also, thicker layer will have a lower heat transfer rate which results in improving interlayer adhesion. That is why printing of specimens with a thicker layer ends up tougher properties. In addition, higher extruder temperature leads to better fusion and adhesion of extruded layers on the solid layers. Infill percentage which determines interior solidity of the printed parts, however, has less influence in the strength of parts which somewhat associated to the solid surface of specimens.

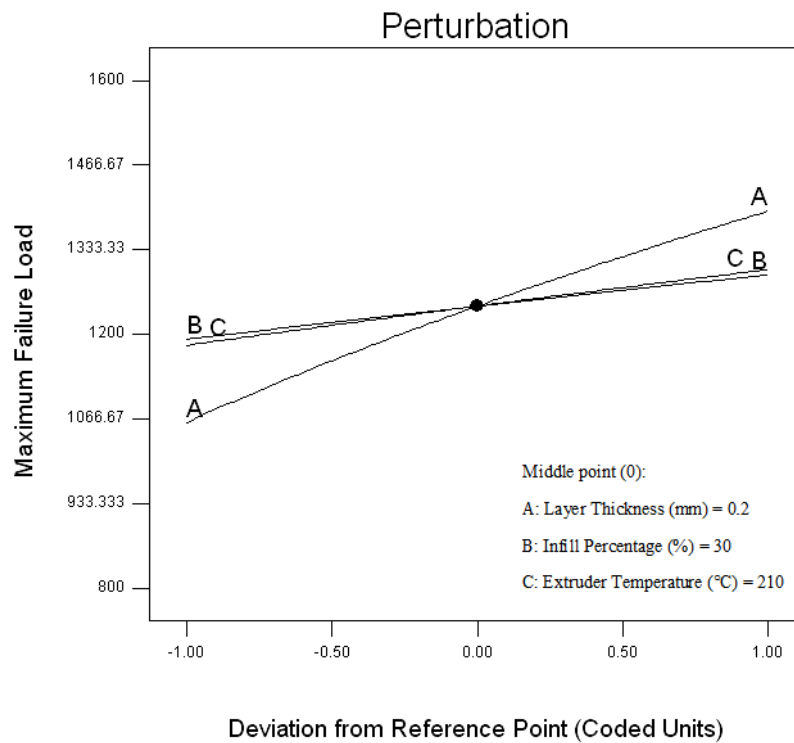


Fig. 6. Perturbation plot of maximum failure load

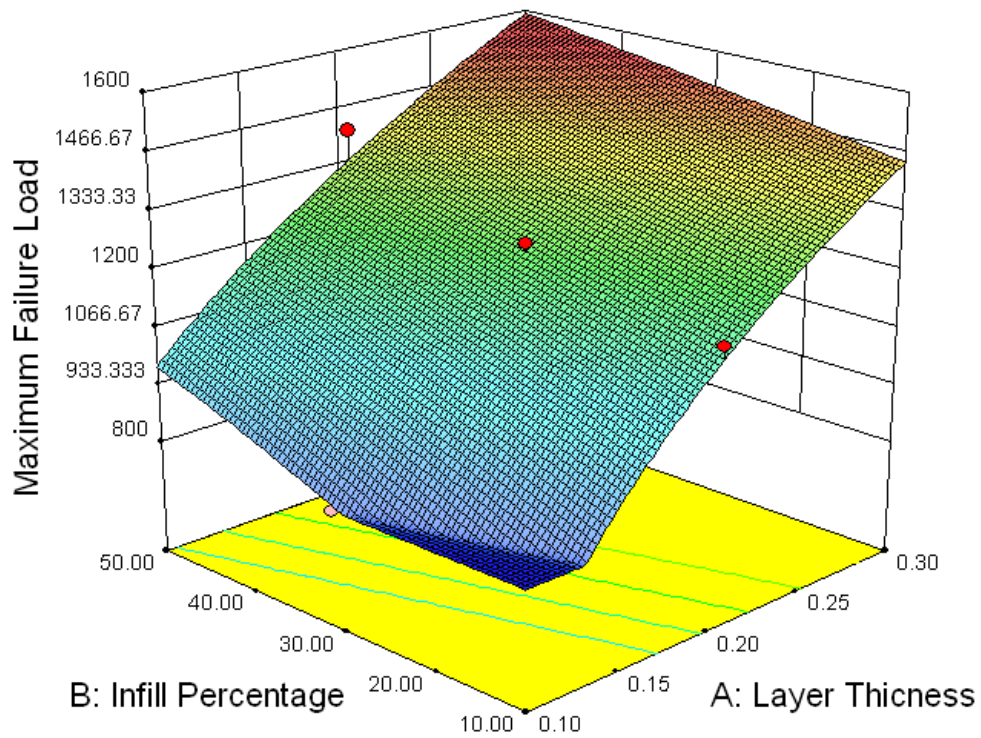


Fig. 7. 3D surface plot of maximum failure load in terms of layer thickness and infill percentage

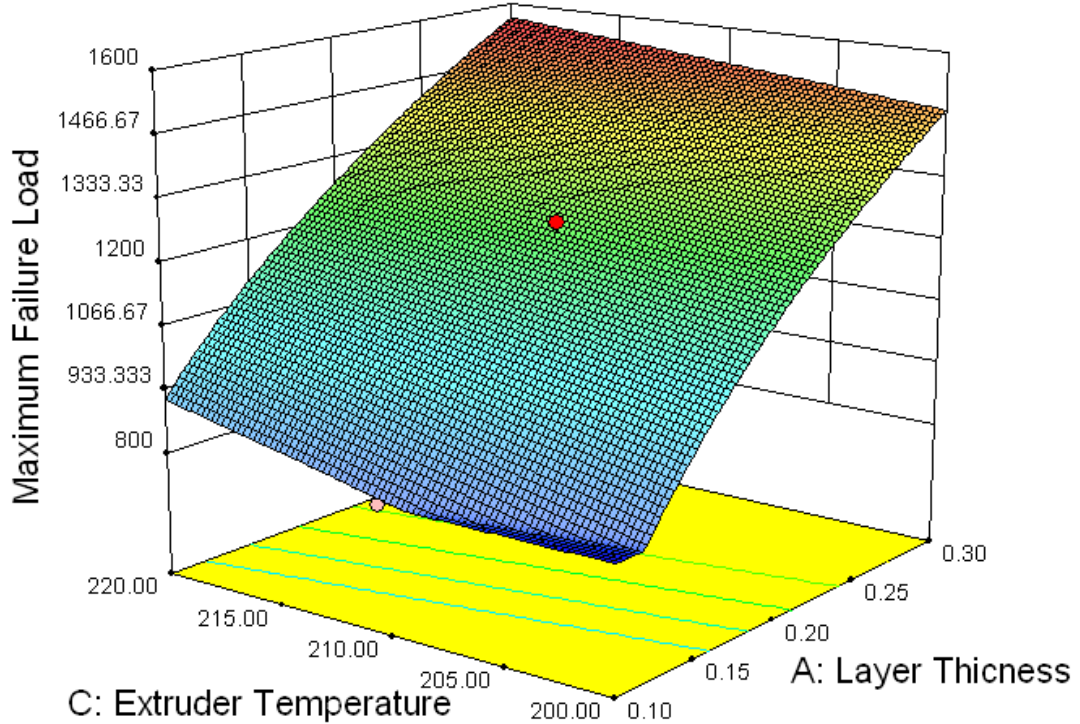


Fig. 8. 3D surface plot of maximum failure load in terms of layer thickness and extruder temperature

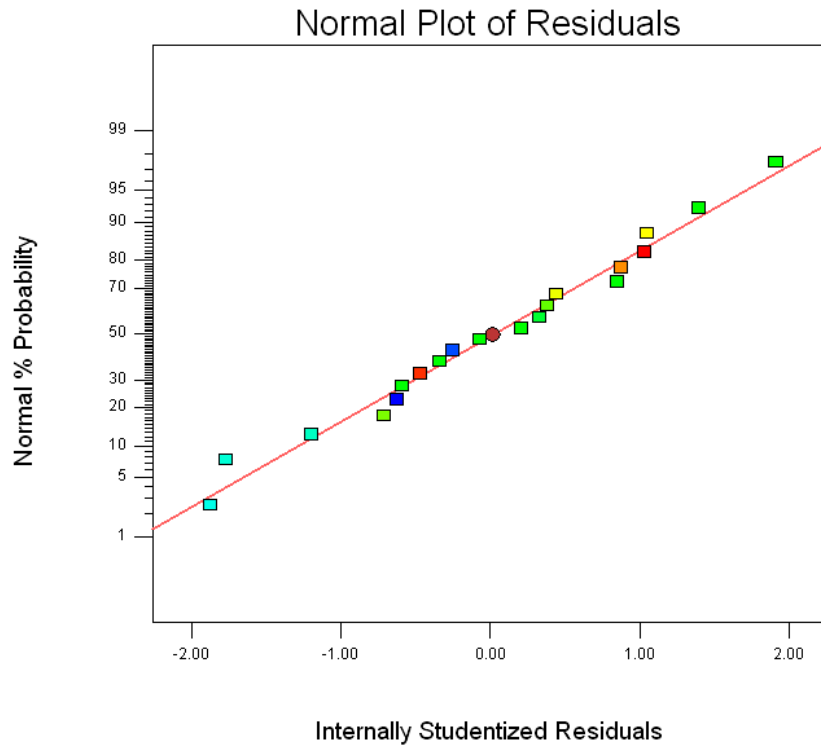


Fig. 9. The normal plot of residuals of failure load

3.2. Elongation at Break

ANOVA table indicates that layer thickness is the dominant controlled variable for elongation at break. In addition, the interaction of infill percentage and extruder temperature has a striking effect on elongation at break. Table 7 demonstrates the ANOVA results of elongation at break.

Table 7. Analysis of variance (ANOVA) for elongation at break

<i>Source</i>	<i>Sum of Squares</i>	<i>Df</i>	<i>Mean Square</i>	<i>F Value</i>	<i>p-value</i>
<i>Model</i>	0.096	4	0.024	6.00	0.0043
<i>Layer Thickness(LT)</i>	0.064	1	0.064	15.89	0.0012
<i>Infill Percentage(IP)</i>	3.956E-003	1	3.956E-003	0.99	0.3365
<i>Extruder Temperature(ET)</i>	5.487E-003	1	5.487E-003	1.37	0.2605
<i>(IP) × (ET)</i>	0.023	1	0.023	5.74	0.0301
<i>Residual</i>	0.060	15	4.013E-003		
<i>Lack of Fit</i>	0.022	10	2.217E-003	0.29	0.9540
<i>Pure Error</i>	0.038	5	7.604E-003		
<i>Cor Total</i>	0.16	19			
Adj R-Squared		0.5126	R-Squared		0.6152

Equation (5) represents predictive model of elongation at break in terms of coded factors:

$$(\text{Elongation at Break})^{-1.6} = +0.29 - 0.063 \text{ LT} - 0.016 \text{ IP} - 0.019 \text{ ET} + 0.054 (\text{IP})(\text{ET}) \quad (5)$$

Equation (6) represents predictive model of elongation at break in terms of actual values:

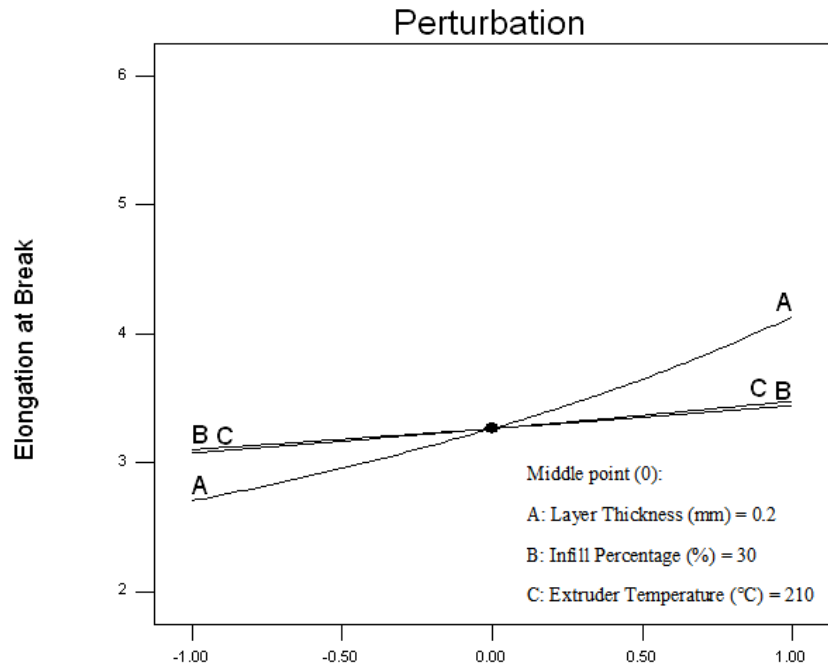
$$(\text{Elongation at Break})^{-1.6} = +4.35291 - 1.26280 \text{ LT} - 0.11421 \text{ IP} - 0.017943 \text{ ET} + 5.36362\text{E-}004 (\text{IP})(\text{ET}) \quad (6)$$

Figure 10 depicts the perturbation plot of elongation at break. Lines A, B, and C show sensitivity of elongation at break to the layer thickness, infill percentage, and extruder temperature respectively. The perturbation plot of elongation at break has a similar trend to perturbation plot of the maximum failure load. However, maximum failure load is more sensitive to layer thickness than the elongation at break. Figure 11 shows the 3D surface plot of elongation at break in terms of layer thickness and infill percentage. Interaction effects of infill percentage and extruder temperature on elongation at break are represented in Fig. 12. It is realized from Fig. 12 that increasing infill percentage at high temperatures results in decreasing elongation at the break; however, increasing infill percentage at low temperatures leads to increasing elongation at break. While low extruder temperatures have a remarkable effect on elongation at break it does not have much influence on maximum failure load. The figure also implies the other way to enhance elongation at break is to increase extruder temperature at low infill percentages. The elongation at break has two maximum in the design space where the infill percentage is maximum and extruder temperature is minimum and where the infill percentage is minimum, and extruder temperature is maximum.

The infill has a honeycomb pattern, and infill percentage specifies density of the pattern. When the infill percentage is maximum, it can be conceived that honeycomb internal pattern can facilitate the redistribution of localized stresses to endure stress concentrations to undergo more plastic deformation.

Mechanical properties of printed parts also depend on the sturdy interlayer adhesion of plastic strings. The extruder puts a string on a layer which is already cooled down to a remarkable lower temperature than the temperature of the extruded string. The difference in temperatures for each layer will cause strings to not fuse thoroughly together. If these strings do not fuse perfectly, it is rational to suppose that the part will have a brittle fracture. The time required to extrude inside layers is dependent on the infill percentage, and thus lower infill percentage leads to lower building time for an inside layer. Therefore, in the production of specimens with lower infill percentage, there is less time to heat transfer and less difference in temperatures which ends in better interlayer adhesion between plastic strings.

The mechanism of fracture can be evaluated by fracture energy which is characterized by maximum failure load and elongation at break. All in all, fracture phenomena in 3D printed parts mainly depends on the interlayer bond strength. Enhancement of the interlayer bond strength results in higher fracture energy which directly determines the mechanism of fracture. An internal pattern which can facilitate the redistribution of localized stresses and build parameters which make a well-built interlayer adhesion leads to higher fracture energy and therefore a tough or ductile fracture.



Deviation from Reference Point (Coded Units)
 Fig. 10. Perturbation plot of elongation at break

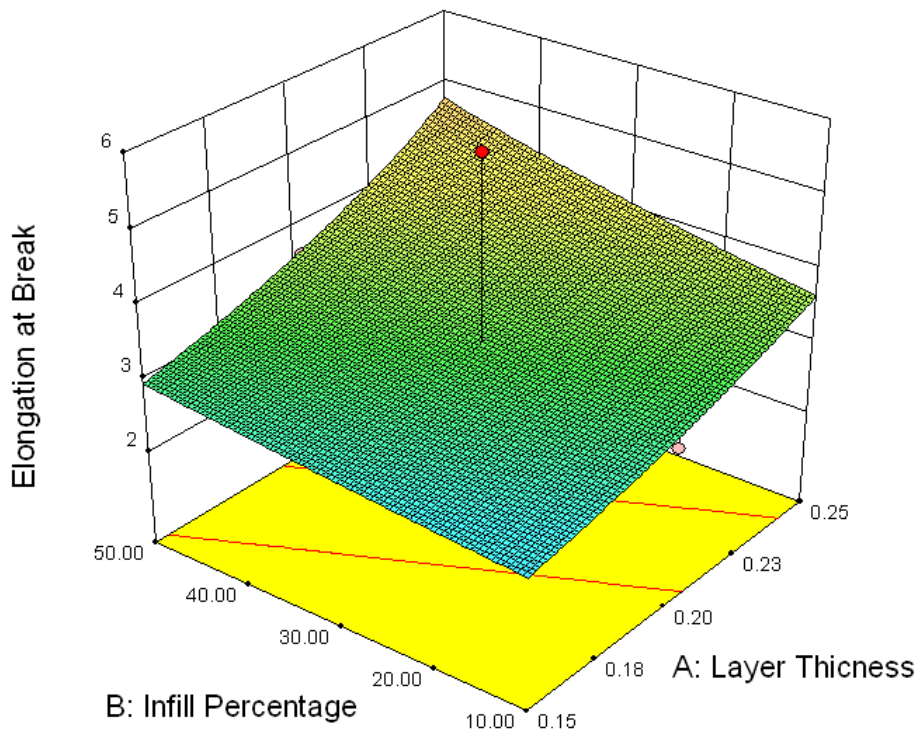


Fig. 11. 3D surface plot of elongation at break in terms of layer thickness and infill percentage

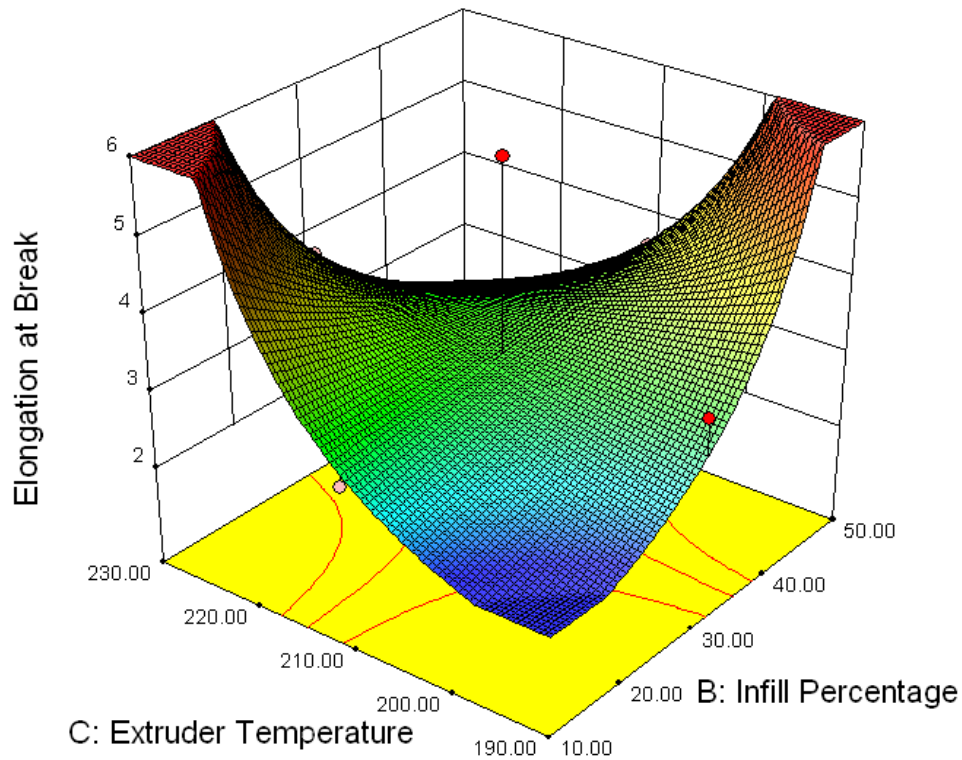


Fig. 12. 3D surface plot of elongation at break in terms of infill percentage and extruder temperature

3.3. Part Weight

ANOVA table reveals that layer thickness and infill percentage are the most substantial controlled variables for part weight. Table 8 demonstrates the ANOVA results of part weight.

Table 8. Analysis of variance (ANOVA) for part weight

<i>Source</i>	<i>Sum of Squares</i>	<i>Df</i>	<i>Mean Square</i>	<i>F Value</i>	<i>p-value</i>
<i>Model</i>	77.74	6	12.96	469.01	< 0.0001
<i>Layer Thickness(LT)</i>	68.92	1	68.92	2494.79	< 0.0001
<i>Infill Percentage(IP)</i>	8.04	1	8.04	290.92	< 0.0001
<i>Extruder Temperature(ET)</i>	0.15	1	0.15	5.54	0.0349
<i>(LT) × (IP)</i>	0.24	1	0.24	8.70	0.0113
<i>(LT) × (EI)</i>	0.3	1	0.3	10.82	0.0059
<i>IP²</i>	0.092	1	0.092	3.31	0.0918
<i>Residual</i>	0.36	13	0.028		
<i>Lack of Fit</i>	0.32	8	0.040	5.04	0.0457
<i>Pure Error</i>	0.040	5	7.921E-003		
<i>Cor Total</i>	78.10	19			

Adj R-Squared	0.9933	R-Squared	0.9954
---------------	--------	-----------	--------

Equation (7) expresses predictive model of part weight in terms of coded factors:
 $(\text{Part Weight})^{1.38} = +17.32 + 2.08 \text{ LT} + 0.71 \text{ IP} + 0.098 \text{ ET} - 0.17 (\text{LT})(\text{IP}) + 0.19 (\text{LT})(\text{ET}) + 0.58 \text{ IP}^2$ (7)

Equation (8) expresses predictive model of part weight in terms of actual values:
 $(\text{Part Weight})^{1.38} = +19.51650 - 29.29224 \text{ LT} + 0.10538 \text{ IP} - 0.067549 \text{ ET} - 0.34657 (\text{LT})(\text{IP}) + 0.38666 (\text{LT})(\text{ET}) + 5.80039 \text{E-}004 \text{ IP}^2$ (8)

Excellent R-Squared and adjusted R-Squared of the predictive model confirms that model is immensely reliable. As the coded equation reveals layer thickness and infill percentage coefficients are much higher than the extruder temperature coefficient. Nonetheless, the influence of honeycomb infill percentage on the part weight is almost one-third of the layer thickness. Due to the small size of the tensile test specimen and the number of tops and solid bottom layers honeycomb internal pattern constitutes a small part of the specimen. However, this interior part would be greater in larger products. In addition, the equation indicates that interactions of parameters are negligible. Figure 13 depicts the perturbation plot of part weight. As the figure discloses part weight is more sensitive to layer thickness. It is evident that part weight is not so sensitive to extruder temperature. Figure 14 demonstrates the effects of layer thickness and infill percentage on part weight. It is observed that increasing infill percentage at lower layer thickness results in tangible changes in part weight. Figure 15 shows the effects of layer thickness and extruder temperature on part weight.

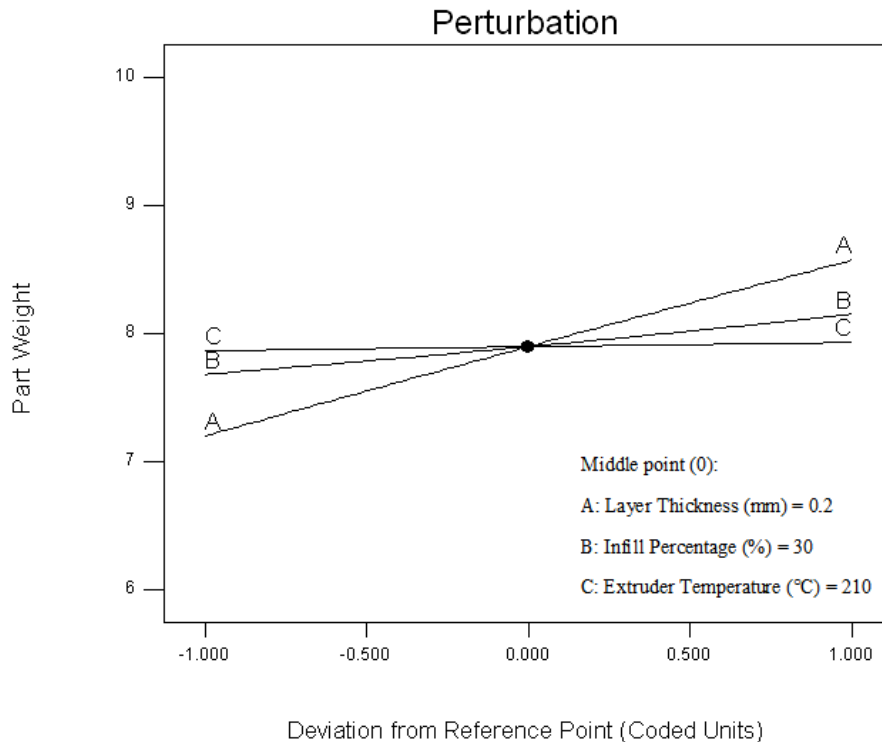


Fig. 13. Perturbation plot of part weight

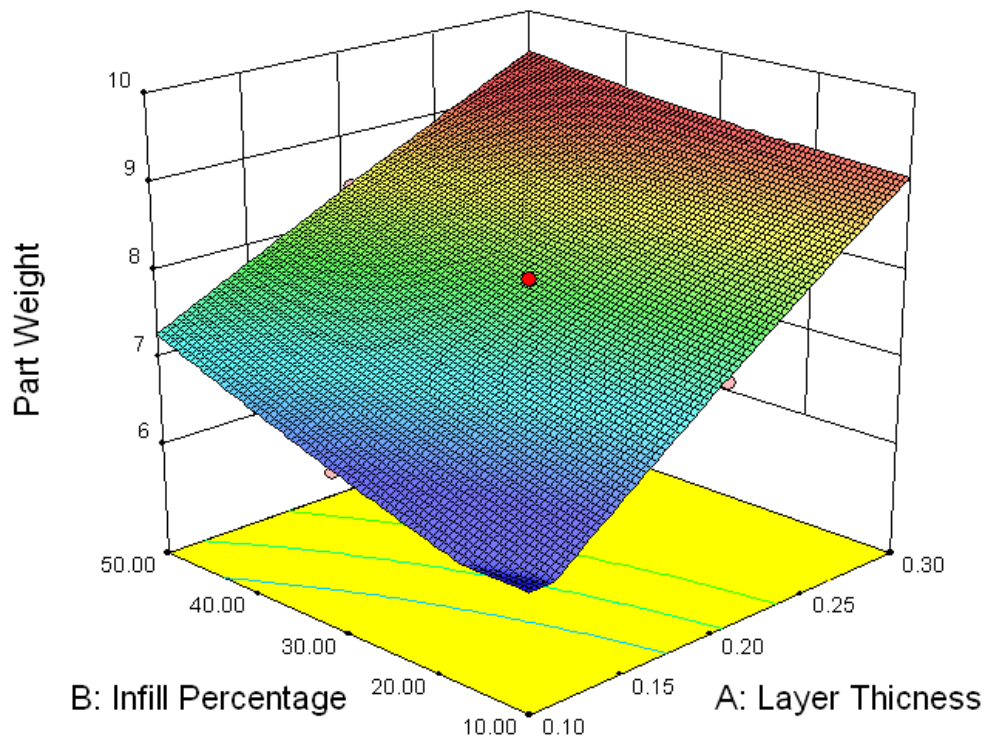


Fig. 14. 3D surface plot of part weight in terms of layer thickness and infill percentage

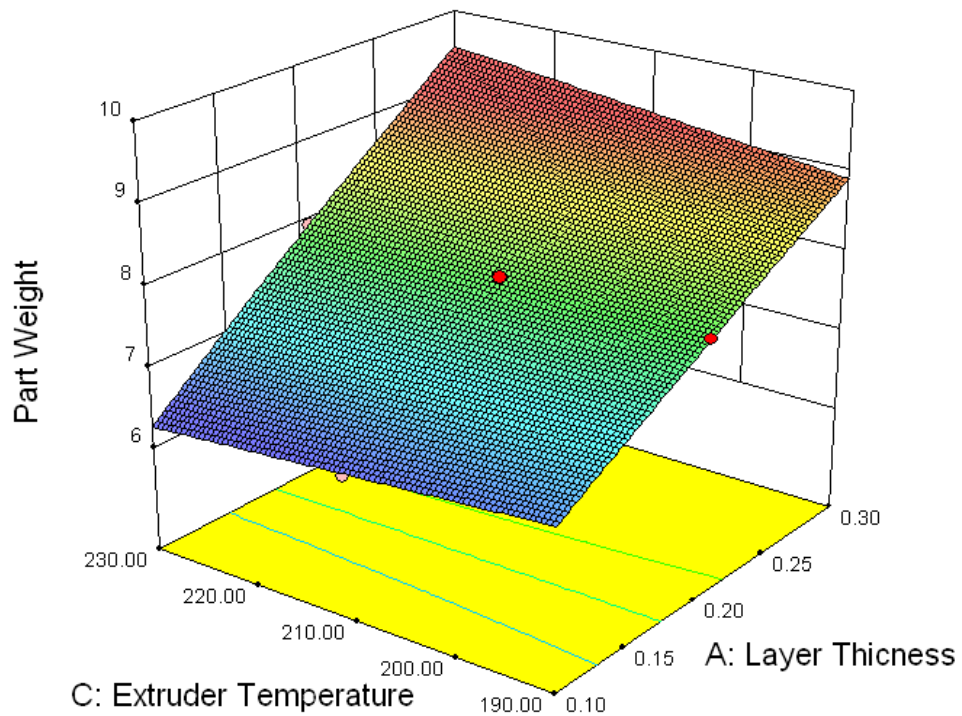


Fig. 15. 3D surface plot of part weight in terms of layer thickness and extruder temperature

3.4. Build Time

ANOVA table indicates that layer thickness and infill percentage are major controlled variables for the build time. In addition, the square of extrusion temperature has a significant effect on build time. Table 9 demonstrates the ANOVA results of build time.

Table 9. Analysis of variance (ANOVA) for build time

<i>Source</i>	<i>Sum of Squares</i>	<i>Df</i>	<i>Mean Square</i>	<i>F Value</i>	<i>p-value</i>
<i>Model</i>	1.088E-005	5	2.176E-006	1498.39	< 0.0001
<i>Layer Thickness(LT)</i>	1.061E-005	1	1.061E-005	7305.05	< 0.0001
<i>Infill Percentage(IP)</i>	2.373E-007	1	2.373E-007	163.42	< 0.0001
<i>IP²</i>	8.043E-009	1	8.043E-009	5.54	0.0337
<i>ET²</i>	3.050E-008	1	3.050E-008	21.00	0.0004
<i>Residual</i>	2.033E-008	14	1.452E-009		
<i>Lack of Fit</i>	2.033E-008	9	2.259E-009		
<i>Pure Error</i>	0.000	5	0.000		
<i>Cor Total</i>	1.090E-005	19			
Adj R-Squared		0.9975	R-Squared		0.9981

Equation (9) is predictive model of build time in terms of coded factors:

$$(\text{Build Time})^{-1.61} = +3.259\text{E-}003 + 8.142\text{E-}004\text{LT} - 1.218\text{E-}004\text{IP} + 1.747\text{E-}005 \text{IP}^2 + 3.402\text{E-}005 \text{ET}^2 \quad (9)$$

Equation (10) is predictive model of build time in terms of actual values:

$$(\text{Build Time})^{-1.61} = +0.015527 + 0.016284 \text{LT} - 2.26600\text{E-}005 \text{IP} - 1.42874\text{E-}004 \text{ET} + 1.74706\text{E-}007 \text{IP}^2 + 3.40177\text{E-}007 \text{ET}^2 \quad (10)$$

The predictive model is still so reliable because of high values of R-Squared and adjusted R-Squared. As the equation reveals, the layer thickness coefficient is higher than infill percentage coefficient. Figure 16 depicts the perturbation plot of build time. Moreover, the figure displays build time is extremely sensitive to layer thickness. The build time decreases meaningfully with increasing layer thickness and increases slightly with increasing infill percentage. It can be explained that with increasing layer thickness the slicer software divides part thickness into fewer sections and therefore the build time is immensely affected by layer thickness. Moreover, with increasing infill percentage the nozzle should scan more internal honeycomb pattern lines at defined sections which takes more time. Figure 17 demonstrates effects of layer thickness and infill percentage on build time.

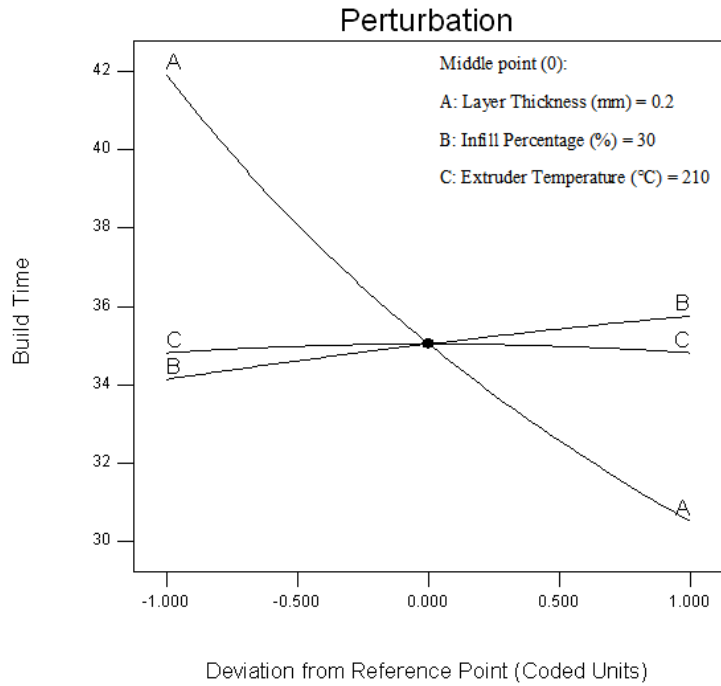


Fig16. Perturbation plot of build time

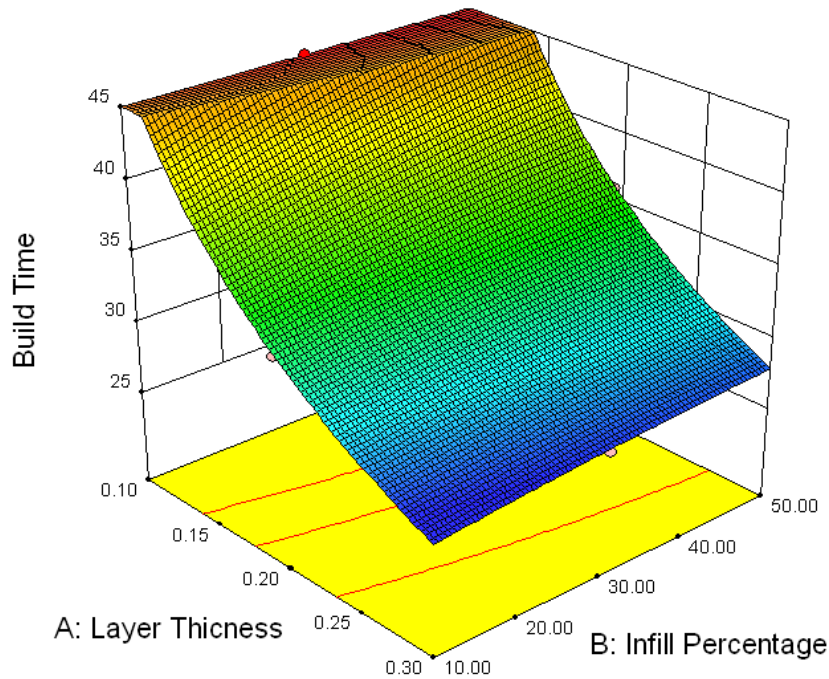


Fig. 17. 3D surface plot of build time in terms of layer thickness and infill percentage

4. Numerical Optimization

Tow criteria are considered for numerical optimization. Table 10 displays the first and second criteria for numerical optimization. The first criterion aims to increase the mechanical strength of 3D printed parts by boosting the maximum failure load. Adequate mechanical strength is regarded as the key characteristic of many industrial, household, and even artistic components. The second criterion is to concurrently achieve maximum failure load and elongation at break and minimum part weight and build time. In addition, different importance is applied to the responses to the second

criterion. The importance of the responses is influential in calculating optimal solutions. The maximum failure load is the most important response and then build time is considered a second important response. Elongation at break and part weight, however, have the lowest values of the importance as shown in Table 10. The objective of optimization based on second criteria is to attain strong parts with a plastic deformation capability at the least possible build time with a reasonable weight. The optimized process parameters to achieve the first and second optimization criterion are shown in Table 11. Optimum solutions take advantage of a high level of desirability. Figure 18 shows the overlay plot which is comprised of contour plots from each response laid on top of each other. On each contour plot, regions which do not meet significations are greyed-out. The remained yellow region defines the final optimal region of input parameters. The overlay plot suggests an adequate process window to build optimal 3D printed parts.

Table 10 Constraints and criteria of input parameters and responses.

Parameters/Responses		Name	Goal	Lower limit	Upper limit	Lower Weight	Upper Weight	Importance
parameters		Layer Thickness	is in rang	0.1	0.3	1	1	-
		Infill Percentage	is in rang	10	50	1	1	-
		Extruder Temperature	is in rang	190	230	1	1	-
Responses	Criteria 1	Maximum Failure Load	maximize	711.2	1545.1	1	1	3
		Elongation at Break	is in rang	2.1663	6.2812	1	1	3
		Part Weight	is in rang	6.45	9.14	1	1	3
		Build time	is in rang	27	54	1	1	3
	Criteria 2	Maximum Failure Load	maximize	711.2	1545.1	1	1	3
		Elongation at Break	maximize	2.1663	6.2812	1	1	1
		Part Weight	minimize	6.45	9.14	1	1	1
		Build time	minimize	27	54	1	1	2

Table 11 Predicted optimum results and experimental validation

solution	Optimum input parameters				Desirability	Output responses			
	LT	IP	ET			Maximum Failure Load (N)	Elongation at break (%)	Part Weight (gr)	Build Time (min)
1	0.27	36.47	226.62	0.98	Actual	1521	5.1253	8.98	31
					Predicted	1558.93	4.2723	9.1195	29.05
					Error%	-2.49%	16.5%	-1.55%	6.29%
2	0.23	16.86	230	0.752	Actual	1437	7.9825	8.42	32
					Predicted	1376.77	9.404	8.1759	30.69
					Error%	4.19%	-17.8%	2.89%	4.09%

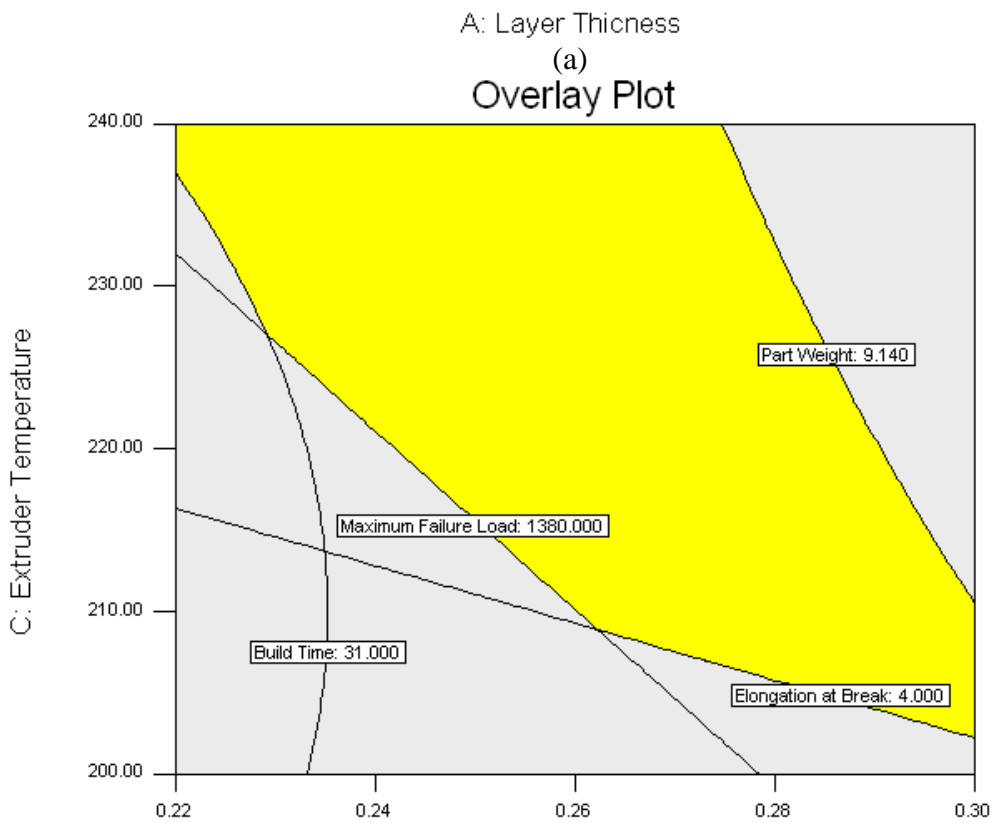
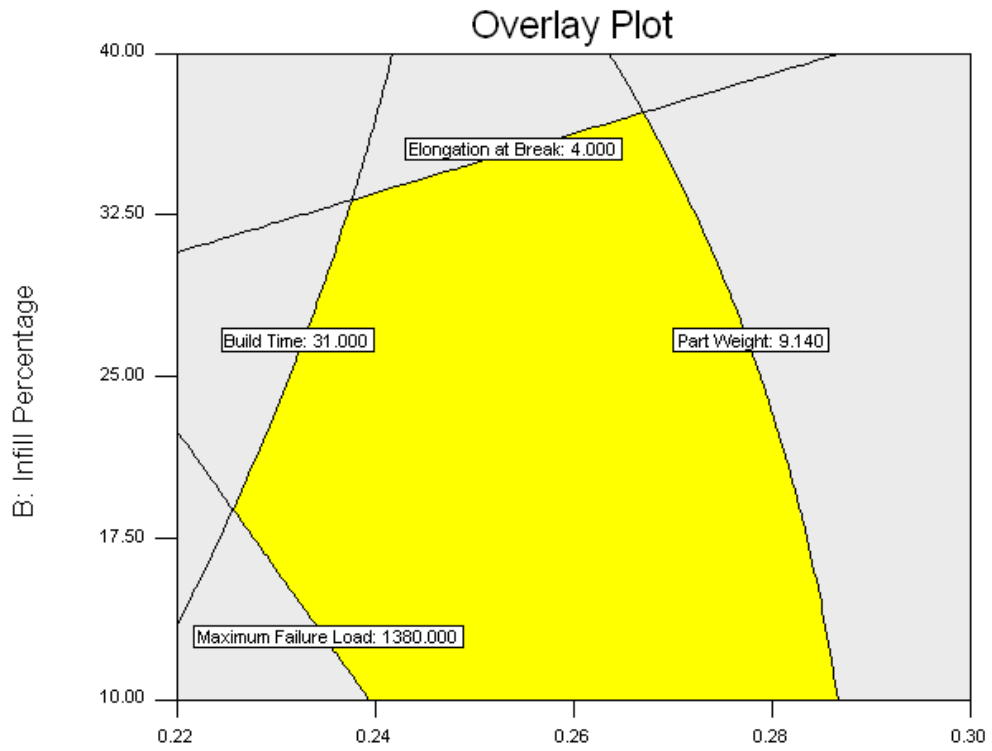


Fig. 18. Overlay plots in terms of (a) layer thickness and extruder temperature (b) layer thickness and infill percentage.

In the final experiment, a tensile test specimen is produced by FDM machine setting %100 infill percentage to compare mechanical properties, part weight, and build time of the filled specimen with optimized specimens. Table 12 compares results of the optimized specimen and filled specimen. The results indicate that optimized specimen promisingly has higher maximum failure load, lower part weight, and shorter build time. Figure 19 represents Force- Extension diagram of the specimen with a %100 infill percentage.

Table 12 Comparison of the optimized specimen with a full specimen

Specimen	Input parameters			Output responses			
	LT	IP	ET	Maximum Failure Load (N)	Elongation at break (%)	Part Weight (gr)	Build Time (min)
Optimized	0.27	36.47	226.62	1521	5.1253	8.98	31
Full	0.27	100	226.62	1410.2	5.3679	10.93	34

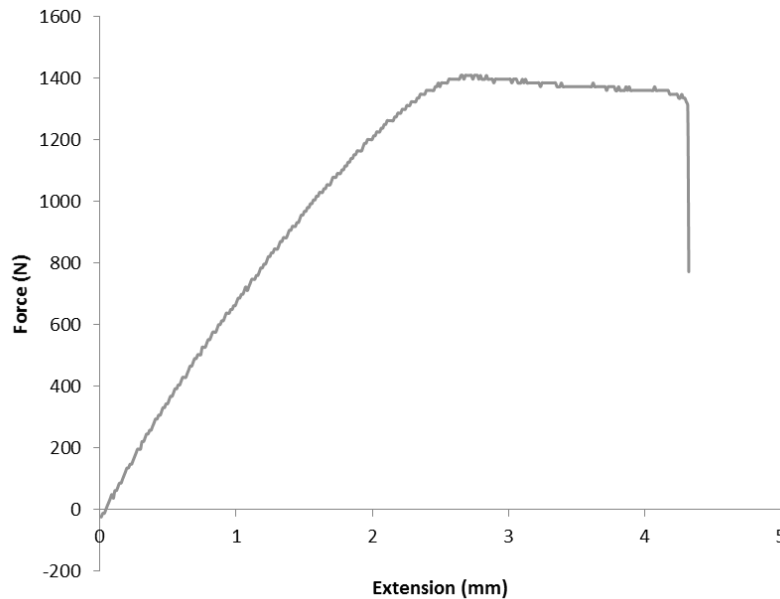


Fig. 19. Extension-Force diagram of the specimen with %100 infill percentage

5. Conclusions

In this research, the FDM process was investigated to enhance mechanical properties and to reduce build time and part weight as far as possible. In addition, effects of Layer thickness (LT), infill percentage (IP) and extruder temperature (ET) on maximum failure load (N), elongation at break (%), part weight (gr), and build time (min) were evaluated by RSM. The following conclusions are mentioned:

1. Honeycomb internal pattern is the adequate internal fill pattern to manufacture low weight PLA components with the ability to undergo slight deformation.

2. Printed tensile test specimens with higher maximum failure load and elongation at break characterize tough fracture. However, sudden brittle fracture is usually observed in PLA specimens at elastic limit and in lower failure load.
3. Increasing layer thickness leads to a positive impact on the strength of specimens and build time, while, results in increasing part weight.
4. Results unveil that infill percentage is the second major parameter influencing part characteristics.
5. It could be inferred that increasing infill percentage at low extruder temperatures and increasing extruder temperature at low infill percentages end up producing more tough specimens because of boosting elongation at break.
6. The optimized printed PLA specimen with almost 9 (gr) weight can resist more than 1500 (N).
7. There is no need to fill inside of 3D printed parts because it was unveiled that optimized specimen has superior mechanical properties, less part weight, shorter build time, and therefore lower production costs than the filled specimen.

References

- [1] Mikell P. Groover. 2010. *Fundamentals of Modern Manufacturing: Materials, Processes, and Systems*. 4th edition. John Wiley & Sons, Inc.
- [2] I. Gibson, D. Rosen, B. Stucker. 2015. *Additive Manufacturing Technologies: 3D Printing, Rapid Prototyping, and Direct Digital Manufacturing*. 2nd edition. Springer
- [3] Sung-Hoon Ahn, Michael Montero, Dan Odell, Shad Roundy, Paul K. Wright, 2002, Anisotropic material properties of fused deposition modeling ABS, *Rapid Prototyping Journal*, 8(4), 248 – 257
- [4] Xinhua Liu, Mingshan Zhang, Shengpeng Li, Lei Si, Junquan Peng, Yuan Hu. 2017. Mechanical property parametric appraisal of fused deposition modeling parts based on the gray Taguchi method, *The International Journal of Advanced Manufacturing Technology*, 89(5-8), 2387
- [5] Guoying Dong, Grace Wijaya, Yunlong Tang, Yaoyao Fiona Zhao. 2018. Optimizing process parameters of fused deposition modeling by Taguchi method for the fabrication of lattice structures, *Additive Manufacturing*, 19, 62–72
- [6] Shahrain Mahmood, A.J. Qureshi, Didier Talamona. 2018. Taguchi based process optimization for dimension and tolerance control for fused deposition modelling, *Additive Manufacturing*, <https://doi.org/10.1016/j.addma.2018.03.009>
- [7] P. M. Pandey, K. Thrimurthulu & N. Venkata Reddy, 2004. Optimal part deposition orientation in FDM by using a multicriteria genetic algorithm, *International Journal of Production Research*, 42(19), 4069-4089
- [8] LM Galantucci, F Lavecchia, G Percoco, 2010. Quantitative analysis of a chemical treatment to reduce roughness of parts fabricated using fused deposition modelling, *CIRP Annals- manufacturing technology*, 59 (1), 247-250
- [9] AK Sood, RK Ohdar, SS Mahapatra. 2012. Experimental investigation and empirical modelling of FDM process for compressive strength improvement, *Journal of Advanced Research*, 3, 81-90
- [10] Venkata Rao, Dhiraj P. Rai. 2016. Optimization of fused deposition modelling process using teaching-learning based optimization algorithm, *Engineering Science Technology an International Journal*, 19(1) 587-603

- [11] Saroj Kumar Padhi, Ranjeet Kumar Sahu, S. S. Mahapatra, Harish Chandra Das, Anoop Kumar Sood, Brundaban Patro, A. K. Mondal. 2017. Optimization of fused deposition modeling process parameters using a fuzzy inference system coupled with Taguchi philosophy, *Advances in Manufacturing*, 5 (3), 231–242
- [12] Julien Gardan, Ali Makke, Naman Recho. 2018. Improving the fracture toughness of 3D printed thermoplastic polymers by fused deposition modeling, *International Journal of Fracture*, 210 (1–2), 1–15
- [13] Anhua Peng, Xingming Xiao, Rui Yue. 2014. Process parameter optimization for fused deposition modeling using response surface methodology combined with fuzzy inference system, *The International Journal of Advanced Manufacturing Technology*, 73 (1–4), 87–100
- [14] Nithin Sajan, T.D.John, Sivadasan.M, N. K Singh. 2018. An investigation on circularity error of components processed on Fused Deposition Modeling (FDM), *Materials Today: Proceedings* 5, 1327–1334
- [15] Rinoj Gautam, Sridhar Idapalapati, Stefanie Feih. 2018. Printing and characterisation of Kagome lattice structures by fused deposition modelling, *Materials and Design*, 137, 266–275
- [16] F Ning, W Cong, J Wei, S Wang. 2015. Additive Manufacturing of CFRP Composites Using Fused Deposition Modeling: Effects of Carbon Fiber Content and Length, *ASME 2015 International Manufacturing Science and Engineering Conference*, Charlotte, North Carolina, USA, June 8–12
- [17] Plymill. Austin; Minneci. Robert; Greeley. Duncan Alexander; and Gritton. Jack. 2016. Graphene and Carbon Nanotube PLA Composite Feedstock Development for Fused Deposition Modeling. . University of Tennessee Honors Thesis Projects. http://trace.tennessee.edu/utk_chanhonoproj/1955
- [18] Ivanova O, Williams C, Campbell T. 2013. Additive manufacturing (AM) and nanotechnology: promises and challenges. *Rapid Prototyp*, 19 (5), 353–64.
- [19] AshishGupta, Alisha kate, Mamta Dhakad, Chandra Prakash Sharma M.K. Ghosh. 2014. A Review of Rapid Manufacturing and Rapid Tooling of FDM Based Material. *International Journal of Emerging Technology & Research*. 1(7), 62-66
- [20] Moradi, M, Mehrabi, O, Azdast, T, Benyounis, KH. Y. 2017 Enhancement of low power CO2 laser cutting process for injection molded polycarbonate. *Optics & Laser Technology* 96, 208–218.
- [21] Moradi M, Mohazabpak A. 2018. Statistical modelling and optimization of laser percussion micro-drilling on Inconel 718 sheet using response surface methodology. *Journal of lasers in Engineering*, 39(9-6). 313-331
- [22] M. Moradi and E. Golchin. 2017. Investigation on the Effects of Process Parameters on Laser Percussion Drilling Using Finite Element Methodology; Statistical Modelling and Optimization. *Latin American Journal of Solids and Structures*, 14(3), pp 464-484.
- [23] M. Moradi, H Abdollahi. 2018. Statistical Modelling and Optimization of the Laser Percussion Microdrilling of Thin Sheet Stainless Steel. *Journal of lasers in Engineering*. 40(1-2).
- [24] Y F Buys, A N A Aznan, H Anuar. 2017. Mechanical properties, morphology, and hydrolytic degradation behavior of polylactic acid / natural rubber blends. *IOP Conf. Series: Materials Science and Engineering* 290. 012077 doi:10.1088/1757-899X/290/1/012077